

THE ULTRAVIOLET SPECTRUM OF SCORPIUS X-1 AS OBSERVED BY *IUE*: 1978–1988

T. R. KALLMAN

Laboratory for High Energy Astrophysics, Code 665, NASA/Goddard Space Flight Center, Greenbelt, MD 20771

AND

J. C. RAYMOND AND S. D. VRTILEK

Harvard-Smithsonian Center for Astrophysics, 60 Garden Street, Cambridge, MA 02138

Received 1990 March 21; accepted 1990 September 11

## ABSTRACT

The *IUE* observations of Sco X-1 taken prior to 1988 September are summarized. These data are tested for variability associated with orbital motion and for correlations between the various observables. The continuum spectra are fitted to simple models for accretion disk atmospheres which demonstrate that X-ray heating dominates the outer regions of the accretion disk. Various scenarios for producing the observed line strengths and ratios are discussed.

*Subject headings:* stars: accretion — stars: individual (Scorpius X-1) — ultraviolet: spectra — X-rays: binaries

## 1. INTRODUCTION

Sco X-1 is notable among compact sources of X-rays as the brightest point source of extrasolar X-rays. It is also considered to be the prototype of the class of binary X-ray sources with low-mass ( $\leq 1 M_{\odot}$ ) companion stars (hereafter called LMXRBs). As such, it is important to our understanding of such diverse issues as quasi-periodic and chaotic phenomena, the late stages of binary star evolution, and the magnetic field geometry of neutron stars.

X-ray observations of Sco X-1, carried out by many experiments, have succeeded in measuring the X-ray spectrum from  $\sim 1$  to 100 keV, and the variability behavior over a range of time scales from  $\sim 10^{-3}$  to  $\sim 10^8$  s. In spite of the wealth of observational data on the X-ray properties of Sco X-1 there remain varying interpretations of the spectral shape and of the physical mechanisms and emission sites (e.g., White, Stella, Parmar 1988).

In wavelength bands other than X-rays, Sco X-1 has been extensively observed (e.g., Canizares et al. 1975 and references therein), but there is less agreement on the most probable physical model for the emission than there is for the X-ray emission. In the case of the ultraviolet, this is partly due to the fact that less than half of the existing data have been analyzed and published. In this paper we analyze and discuss the results of ultraviolet observations of Sco X-1 taken prior to 1989 using the *IUE* satellite, together with some of the implications of these observations for theories of Sco X-1 and the relation between the UV and other wavelength bands. A more recent set of UV observations of Sco X-1 was obtained as part of a multiwavelength observing campaign during 1989; these will be published elsewhere (Vrtilek et al. 1990).

## 2. DATA ANALYSIS

2.1. *The Data*

The data used in this analysis represent all of the available spectra of Sco X-1 taken by the *International Ultraviolet Explorer* (*IUE*) between the time of its launch (1978) and 1988 September. A description of the instrument is given by Boggess et al. (1978a, b). With a few exceptions, the data reported here were taken during three observing campaigns:

1978–1979 (during the post-commissioning phase X-ray binary monitoring effort), 1980, and 1984. The data from the first campaign, representing approximately  $\frac{1}{3}$  of the total, have been presented by Willis et al. (1980). A journal of observations is presented in Table 1, sorted according to camera: *IUE* image number, epoch (at the beginning of the exposure), and orbital phase (based on the ephemeris of Gottlieb, Wright, & Liller 1975). Most observations lasted 20–40 minutes. This list contains a total of 79 images, of which 32 were taken with the long-wavelength (2000–3200 Å) cameras and 47 were taken with the short wavelength-(1100–2000 Å) camera. An additional seven images were obtained but were not included in our analysis for various reasons, including incomplete or erroneous data, use of the small aperture, or calibration uncertainties associated with the commissioning phase of the satellite. All except one of these were taken in the low- $(\Delta\lambda \simeq 6 \text{ \AA})$  resolution mode of *IUE*.

2.2. *Analysis*

The data analysis procedure consisted of extraction of flux-calibrated spectra, reddening correction, continuum fitting, and emission line fitting. The data were reduced in a uniform manner using the analysis software of the *IUE* processing system available at the data analysis facility (RDAF) at NASA's Goddard Space Flight Center. Comparison of the results of this analysis for several of the images with those obtained by the Gaussian extraction technique (GEX) developed by Urry & Reichert (1989) find differences which we deem to be small in comparison with the potential systematic errors in these data. This is consistent with the results of Clavel et al. (1990) who performed a thorough comparison of the two techniques in their analysis of the data from the Seyfert galaxy NGC 5548. Data taken between 1978 May and 1979 July were corrected to take into account changes in the instrument calibration since the images were originally extracted. The data were mapped onto a uniform wavelength grid and were calibrated into flux units. Several representative spectra are displayed in Figures 1a and 1b (short-wavelength) and 1c (long-wavelength), together with average spectra. We note that, owing to the highly variable nature of this source, such average spectra are of limited applicability in characterizing the source properties.

TABLE 1  
LIST OF IMAGES, OBSERVATION EPOCH, AND ORBITAL PHASE

Image Number	Julian date JD + 2,440,000	Phase	Image Number	Julian date JD + 2,440,000	Phase
SWP 1444	3629.02	0.33	SWP 22514	5777.77	0.55
SWP 1452	3630.01	0.59	SWP 23424	5889.38	0.30
SWP 1463	3631.23	0.13	SWP 23425	5889.43	0.36
SWP 1470	3631.91	0.00	SWP 23479	5903.35	0.05
SWP 1473	3632.24	0.41	SWP 23480	5903.42	0.14
SWP 1490	3634.39	0.14	SWP 23592	5916.43	0.66
SWP 1491	3634.47	0.25	SWP 23593	5916.48	0.72
SWP 1499	3635.96	0.14	SWP 23594	5916.52	0.78
SWP 1953	3699.51	0.86	SWP 23702	5929.42	0.16
SWP 1954	3699.62	0.00	SWP 23703	5929.47	0.23
SWP 2028	3706.08	0.20	SWP 23704	5929.52	0.29
SWP 2033	3707.06	0.45	LWP 2901	5765.79	0.32
SWP 2039	3707.76	0.33	LWP 2917	5769.77	0.38
SWP 2040	3707.83	0.42	LWP 2947	5773.73	0.41
SWP 2041	3707.88	0.49	LWP 2975	5777.70	0.45
SWP 2048	3708.77	0.62	LWP 2976	5777.75	0.51
SWP 2062	3710.73	0.11	LWP 3728	5889.40	0.32
SWP 2063	3710.81	0.21	LWP 3729	5889.45	0.39
SWP 2064	3710.87	0.28	LWP 3837	5903.39	0.09
SWP 2065	3710.92	0.35	LWP 3930	5916.45	0.69
SWP 2066	3710.99	0.43	LWP 3931	5916.50	0.75
SWP 2076	3711.72	0.37	LWP 4003	5929.39	0.12
SWP 2077	3711.79	0.46	LWP 4004	6295.45	0.06
SWP 2078	3711.85	0.53	LWP 4005	5929.50	0.25
SWP 2079	3711.90	0.59	LWR 1420	3629.09	0.41
SWP 2080	3711.95	0.66	LWR 1431	3631.60	0.61
SWP 4641	3947.89	0.33	LWR 1432	3631.67	0.69
SWP 4642	3947.96	0.42	LWR 1434	3631.95	0.05
SWP 7782	4265.20	0.37	LWR 1446	3634.44	0.21
SWP 8744	4342.66	0.74	LWR 1450	3636.00	0.19
SWP 9417	4422.72	0.44	LWR 1804	3699.55	0.91
SWP 9636	4450.39	0.57	LWR 1846	3707.79	0.38
SWP 9658	4452.62	0.41	LWR 1866	3710.77	0.16
SWP 9677	4454.32	0.57	LWR 1872	3711.76	0.41
SWP 22424	5765.74	0.26	LWR 4028	3947.92	0.37
SWP 22453	5769.73	0.32	LWR 4029	3947.99	0.46
SWP 22485	5773.69	0.36	LWR 6783	4265.23	0.41
SWP 22486	5773.77	0.46	LWR 7496	4342.69	0.79
SWP 22512	5777.67	0.41	LWR 8385	4450.42	0.62
SWP 22513	5777.72	0.48	LWR 8400	4452.58	0.36

NOTES.—Julian date corresponds to the beginning of the exposure. Orbital phase is calculated from the ephemeris of Gottlieb, Wright, & Liller 1975.

### 2.3. Reddening

The data have been corrected for the effects of interstellar reddening by using the extinction curve of Savage & Mathis (1979). We adopt a reddening of  $E(B-V) = 0.3$ , which provides an acceptable fit to the 2200 Å feature and which is consistent with that obtained by previous workers (Willis et al. 1980). Figure 2 displays the dereddened average spectrum in the long-wavelength band (2000–3000 Å) for various different choices of  $E(B-V)$ .

We have also fitted the spectrum in the vicinity of Ly $\alpha$  to a damped absorption profile; the fits are shown in Figure 3. We find the best-fit value of the H I column density to be  $6 \pm 2 \times 10^{21} \text{ cm}^{-2}$ . This corresponds to  $E_{B-V} \simeq 1$  using an average extinction law (Savage & Mathis 1979). However, we do not consider the discrepancy between this and the 2200 Å derived reddening value to be significant, given the uncertainties associated with fitting the wings of Ly $\alpha$ , and given the likely variations in interstellar gas-to-dust ratios.

We note that neither of our reddening estimates are consistent with the (much lower) reddening adopted by Schachter, Filippenko, & Kahn (1989) in their study of optical line emis-

sion from Sco X-1 or with the lower reddening suggested by Knude (1987) on the basis of optical colors of stars in the direction of Sco X-1. While it is conceivable that an anomalous reddening curve with a 2200 Å feature far stronger than normal accounts for this discrepancy, we believe that the low reddening derived by Schachter et al. (1989) results from an incorrect assumption of case B recombination for the He II lines (see below), and that Knude's sample of stars did not extend to great enough distances.

### 2.4. Fits

#### 2.4.1. Continuum

The continuum was fitted by first excluding the regions containing known strong emission lines from the reduced data, and then fitting to a model spectrum using a least-squares procedure. The model spectrum is assumed to be that of an accretion disk and is given by

$$F_{\lambda}^{\text{model}} = (4\pi D^2)^{-1} \int_{R_{\text{min}}}^{R_{\text{max}}} F_{\lambda}^{\text{local}}[T(R)] 2\pi R dR, \quad (1)$$

where  $R$  is the radial variable,  $T(R)$  is the disk photospheric

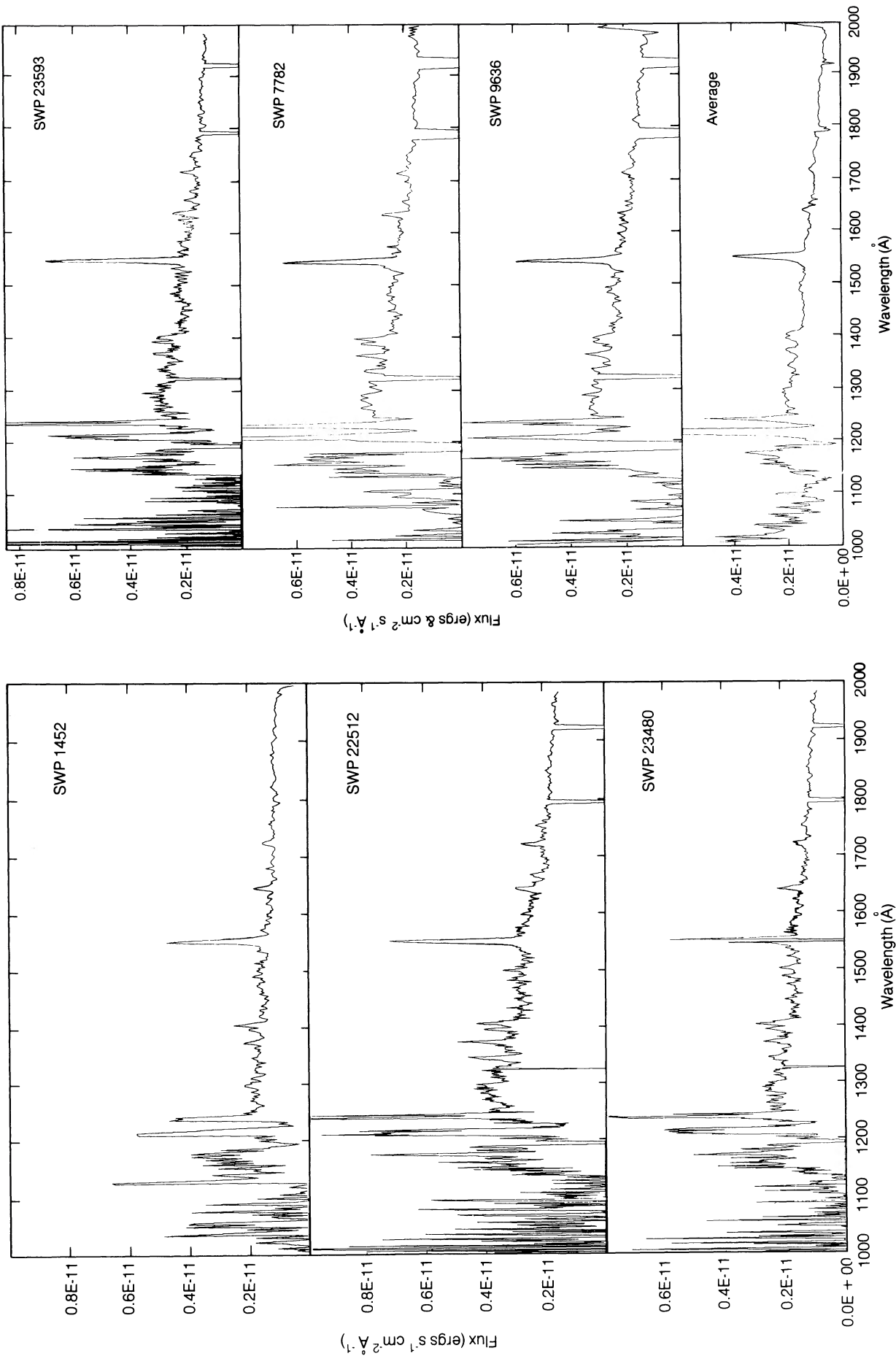


FIG. 1.—Spectra from various *IUE* images plotted against wavelength, including the average spectra.

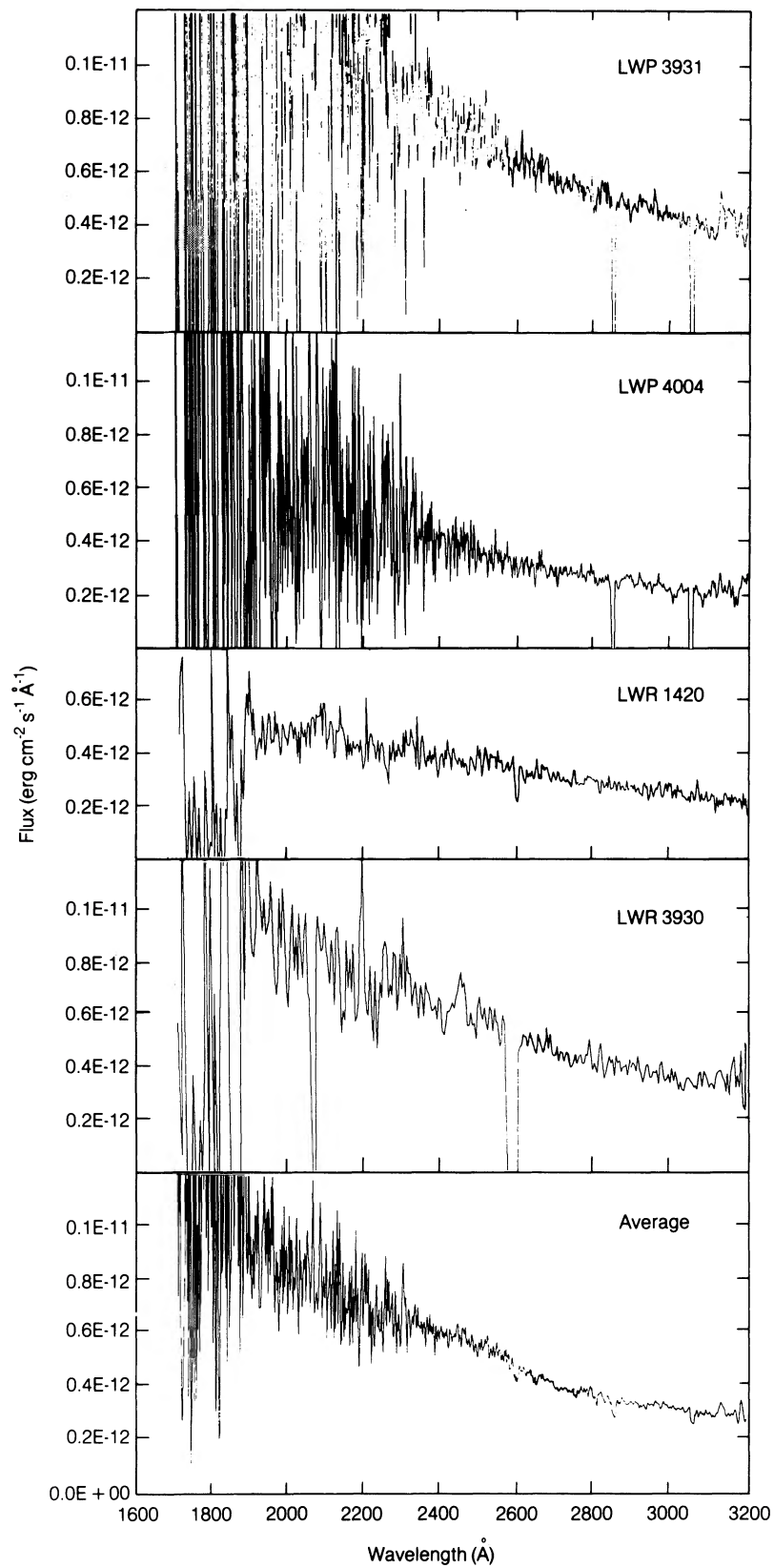


FIG. 1—Continued

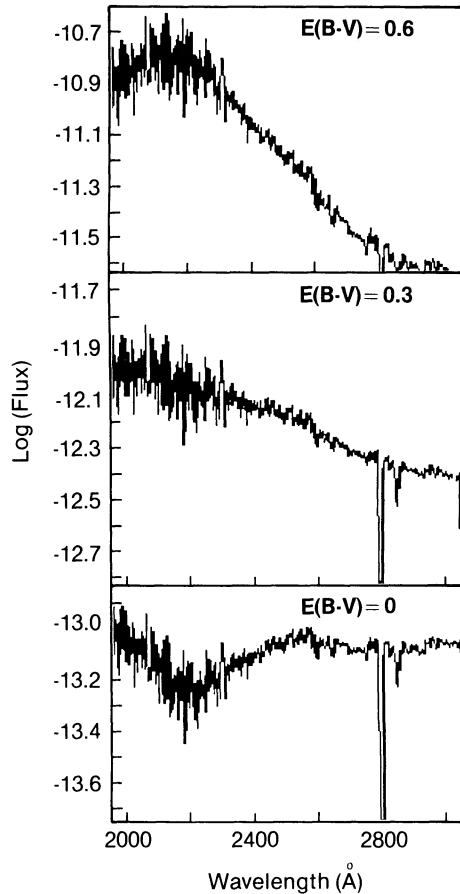


FIG. 2.—Fits to the average spectrum in the long-wavelength band for various choices of reddening,  $E(B-V)$ .

temperature, and  $F_{\lambda}^{\text{local}}$  is the local spectrum radiated by the disk surface. We ignore emission from the X-ray-heated face of the companion star. This has been shown to be a very minor contribution to the UV light in the LMXRB Cyg X-2 (Vrtilek et al., 1989), although it appears to be a significant contribution in the Her X-1/HZ Her system (Howarth & Wilson 1983). As

discussed in the following section, we are unable to detect the orbital modulation which would be expected from a heated companion in the data considered here. Furthermore, we expect an illuminated companion to more nearly resemble a single-temperature blackbody or stellar-type distribution, significantly different from the disk spectral distribution; our success in fitting to disk spectra provides post hoc justification for neglect of companion star heating.

Theoretical calculations of the local disk spectrum are affected by the various and uncertain heating mechanisms which may affect the disk atmosphere (see, e.g., Shaviv & Wehrse 1986) and by the problems of line blanketing and non-LTE conditions familiar from the modeling of stellar atmospheres. In the absence of detailed models for the continuum spectra emitted by accretion disk atmospheres, there are two plausible choices for  $F_{\lambda}^{\text{local}}$ : normal stellar atmospheres or blackbody distributions. Studies of cataclysmic variables have shown that neither of these distributions closely match observations of those accretion disks in detail (Wade 1984). Many of the differences between these two cases, and their effects on the total disk spectra, have been discussed by Vrtilek et al. (1990), who adopt stellar atmospheres in their fitting of the spectra of Cyg X-2. In our models we follow Vrtilek et al. (1990) and adopt the stellar atmospheres from the compilation by Kenyon (1989) when calculating  $F_{\lambda}^{\text{local}}$ . For the purposes of modeling the UV continuum the inner optically thin or Compton-scattering-dominated regions of the disk are unimportant (Shakura & Sunyaev 1973; Eardley et al. 1978).

The disk temperature distribution may be influenced by a variety of factors, including the viscous release of energy by the accreting material and heating by X-rays from the central compact object. Viscosity alone produces a temperature distribution  $T_{\text{acc}}(R) = [3GM\dot{M}/(8\pi\sigma)]^{1/4} R^{-3/4}$ , where  $M$  and  $\dot{M}$  are the central object mass and mass accretion rate, respectively. X-ray illumination produces a temperature distribution  $T_x(R) = [L_x f_x / (4\pi\sigma)]^{1/4} R^{-1/2} = [\dot{M} c^2 \eta / (4\pi\sigma)]^{1/4} R^{-1/2}$ , where  $L_x$  is the X-ray luminosity and  $\eta$  is the accretion efficiency, which we assume to be 0.1. The illumination of the disk by X-rays is parameterized by the factor

$$f_x = (4\pi R^2 F_{x,\text{inc}}) / L_x \quad (2)$$

the ratio of the X-ray flux incident on the disk surface,  $F_{x,\text{inc}}$  to the total available unattenuated X-ray flux at that radius. The quantity  $f_x$  may be regarded as analogous to the “Eddington factor” familiar from the study of stellar atmospheres. If the X-rays are unattenuated and streaming radially outward from a point source at the center of the disk, then  $f_x = \sin \theta$ , where  $\theta$  is the local flaring angle of the disk. On the other hand, if the X-rays are nearly isotropic with the corresponding mean intensity,  $f_x \approx 1$ . There is no *a priori* reason to adopt either of these scenarios, since there is evidence that the disks in LMXRBs are surrounded by X-ray-induced coronas (Begelman & McKee 1983; Begelman, McKee, & Shields, 1983; White & Holt 1982). Such coronas will have temperatures  $\sim 10^7$ – $10^8$  K and optical depths to electron scattering 0.1–1, and so can isotropize the X-rays illuminating the disk. The detailed properties of such a corona, including its radial extent, are somewhat uncertain, although the models of London (1982) suggest that  $f_x \leq 10^{-1}$  for accretion onto a neutron star at a rate less than the Eddington limit.

A consequence of the different temperature dependences of the disk temperatures produced by accretion and X-ray heating, and of the great range of radii spanned by likely disk

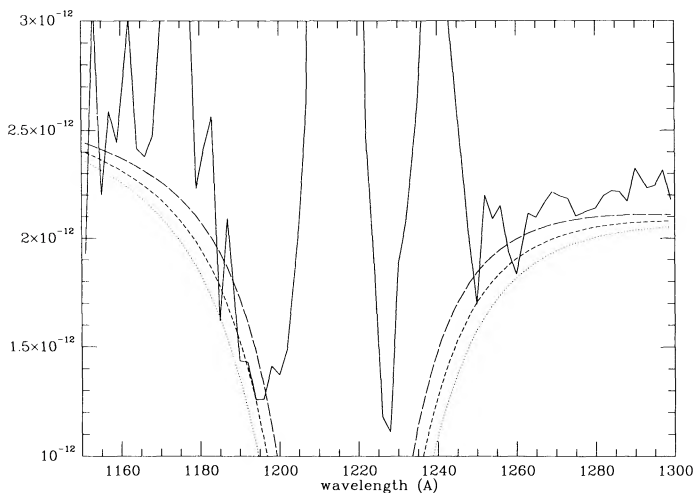


FIG. 3.—Fits to the spectrum in the vicinity of the Ly $\alpha$  line. Solid curve is average observed spectrum; long dashed, short dashed, and dotted curves correspond to absorption by columns of  $6 \times 10^{21} \text{ cm}^{-2}$ ,  $8 \times 10^{21} \text{ cm}^{-2}$ , and  $1 \times 10^{22} \text{ cm}^{-2}$ , respectively.

models, is that X-ray heating is likely to dominate viscous heating at large radii, i.e.,  $R \geq R_{\text{eq}} = 3GM/(2f_x \eta c^2) = 2.2 \times 10^9 \text{ cm } (\eta/0.1)^{-1} (M/M_\odot)(f_x/10^{-3})^{-1}$ . Thus, even for very small values of  $f_x$ , X-ray heating can determine the temperature at large radii and can strongly affect the UV continuum.

The integrated spectrum given by equation (1) will be influenced by the sum of the local spectra from the various disk radii at wavelengths less than those which characterize the outer disk radius,  $\lambda_{\text{out}} \sim hc/\{k \max [T_x(R_{\text{max}}), T_{\text{acc}}(R_{\text{max}})]\}$ . If so, a disk which radiates locally as a blackbody will have  $F_\lambda \sim \lambda^{-7/3}$  if viscous heating dominates and  $F_\lambda \sim \lambda^{-1}$  if X-ray heating (with  $f_x$  constant across the disk surface) dominates. Stellar atmosphere spectra are generally flatter than the blackbody spectra at the corresponding temperature. For  $\lambda \geq \lambda_{\text{out}}$ , the spectrum has a Rayleigh-Jeans slope,  $F_\lambda \sim \lambda^{-5}$ .

In evaluating the model spectrum we assume that Sco X-1 is a  $1 M_\odot$  Eddington-limited neutron star emitting X-rays at  $L = 10^{38} \text{ ergs s}^{-1}$ , implying a distance  $D = 1.4 \text{ Kpc}$  (White, Peacock, & Taylor, 1985). We take the accretion efficiency  $\eta = 0.1$ , so that  $\dot{M} \leq 1.1 \times 10^{18} \text{ g s}^{-1}$ . The free parameters

used to maximize the fit to the observed spectrum include  $f_x$  (assumed to be constant over the disk surface), the mass accretion rate, and the disk outer radius,  $R_{\text{max}}$ .

Some sample fits using stellar atmosphere spectra are displayed in Figure 4a (short-wavelength) and 4b (long-wavelength), including the average spectrum calculated by mapping all spectra onto the same wavelength grid and summing the fluxes in each bin. These spectra, although not labeled, correspond in image number to those shown in Figure 1. The values of  $f_x$ ,  $\dot{M}$  (in units  $1.1 \times 10^{18} \text{ g s}^{-1}$ ) and  $R_{\text{max}}$  (in units of lt-sec,  $3 \times 10^{10} \text{ cm}$ ) for all the various individual spectra are summarized in Table 2A. Note that the mass accretion rate is constrained to be less than the Eddington limit, i.e.,  $\dot{M} \leq 1$  in the units of Table 2A; when this limit is reached (as it often is) X-ray heating is the dominant energy source for the UV-emitting part of the disk. We find in most cases that an acceptable fit is obtained to these choices of model spectra. As shown in Figure 4, the spectral slope in the UV is flatter than  $F_\lambda \sim \lambda^{-7/3}$  expected for viscous-dominated disks. This is consistent with the effects of X-ray heating, but is partially offset by the

TABLE 2A  
DERIVED CONTINUUM PARAMETERS

Image	$\dot{M}$	$f_x$	Optical Error	$R_{\text{max}}$	Image	$\dot{M}$	$f_x$	Optical Error	$R_{\text{max}}$
SWP 1444	1.0	6.9E-04	1.0	3.2	SWP 23425	1.0	1.4E-03	3.5	5.2
SWP 1452	1.0	9.4E-04	3.8	7.2	SWP 23479	1.0	1.2E-03	3.0	4.9
SWP 1463	0.8	9.1E-04	2.2	5.0	SWP 23480	1.0	1.1E-03	2.8	4.7
SWP 1470	1.0	1.0E-03	2.7	4.8	SWP 23592	1.0	1.5E-03	4.4	6.1
SWP 1473	1.0	1.1E-03	3.2	5.5	SWP 23593	1.0	1.4E-03	3.7	5.4
SWP 1490	1.0	9.3E-04	3.7	7.0	SWP 23594	1.0	1.4E-03	5.1	7.1
SWP 1491	1.0	9.3E-04	2.2	4.4	SWP 23702	0.7	8.9E-04	0.5	2.6
SWP 1499	1.0	9.9E-04	2.3	4.4	SWP 23703	0.8	8.3E-04	0.8	2.8
SWP 1953	1.0	8.4E-04	2.2	4.6	SWP 23704	1.0	7.6E-04	1.6	4.0
SWP 1954	1.0	8.8E-04	2.9	5.7	SW average	1.0	1.1E-03	2.9	5.1
SWP 2028	1.0	1.7E-03	6.1	7.6	LWP 2901	0.4	3.0E-03	0.2	1.8
SWP 2033	1.0	1.0E-03	2.8	5.1	LWP 2917	0.5	3.0E-03	0.7	2.1
SWP 2039	1.0	1.3E-03	5.2	8.1	LWP 2947	0.6	3.5E-03	0.3	1.7
SWP 2040	1.0	1.1E-03	4.2	7.1	LWP 2975	1.0	2.8E-03	2.0	2.9
SWP 2041	1.0	1.4E-03	4.0	5.7	LWP 2976	0.4	7.2E-03	1.9	2.9
SWP 2048	1.0	1.1E-03	3.2	5.4	LWP 3728	0.6	2.6E-03	1.8	3.1
SWP 2062	1.0	7.1E-04	0.9	3.0	LWP 3729	1.0	2.4E-03	1.6	2.7
SWP 2063	0.5	1.2E-03	1.0	3.4	LWP 3837	0.6	3.5E-03	1.2	2.4
SWP 2064	1.0	6.4E-04	1.2	3.6	LWP 3931	0.7	3.0E-03	1.0	2.3
SWP 2065	1.0	6.9E-04	1.1	3.3	LWP 4003	0.5	2.8E-03	0.0	1.3
SWP 2066	1.0	7.1E-04	1.8	4.5	LWP 4004	0.9	1.6E-03	0.0	1.3
SWP 2076	0.6	1.1E-03	0.5	2.5	LWP 4005	0.6	3.8E-03	0.0	0.9
SWP 2077	1.0	7.1E-04	1.1	3.3	LWR 1420	0.3	2.8E-03	0.0	1.6
SWP 2078	0.5	1.3E-03	2.4	5.8	LWR 1432	0.3	2.8E-03	1.0	2.9
SWP 2079	1.0	9.3E-04	3.1	5.8	LWR 1434	0.5	1.5E-03	0.7	2.6
SWP 2080	0.8	8.6E-04	0.7	2.7	LWR 1446	0.3	2.8E-03	0.1	1.7
SWP 4641	1.0	1.6E-03	4.8	6.3	LWR 1450	0.3	2.7E-03	1.0	2.9
SWP 4642	1.0	9.0E-04	2.3	4.7	LWR 1846	0.5	3.1E-03	0.7	2.2
SWP 7782	1.0	1.7E-03	3.8	5.1	LWR 1866	0.8	2.1E-03	0.0	1.0
SWP 8744	1.0	1.3E-03	1.9	3.6	LWR 1872	0.5	3.5E-03	0.0	0.8
SWP 9636	1.0	1.6E-03	3.2	4.5	LWR 1953	0.3	2.9E-03	0.1	1.7
SWP 9658	0.8	8.7E-04	0.5	2.5	LWR 3930	0.4	3.3E-03	1.3	2.9
SWP 22424	1.0	8.1E-04	1.3	3.4	LWR 4028	0.5	3.0E-03	0.1	1.6
SWP 22453	1.0	1.1E-03	2.2	4.1	LWR 4029	0.6	3.8E-03	1.6	2.8
SWP 22485	1.0	9.4E-04	1.8	3.8	LWR 6783	0.4	2.6E-03	0.7	2.3
SWP 22486	1.0	1.2E-03	4.2	6.5	LWR 7496	0.6	4.0E-03	0.9	2.2
SWP 22512	1.0	1.9E-03	5.0	5.9	LWR 8385	0.4	3.2E-03	0.0	1.4
SWP 22513	1.0	1.9E-03	4.2	5.2	LWR 8400	0.7	2.1E-03	0.0	1.0
SWP 22514	1.0	2.0E-03	4.4	5.3	LW average	0.4	3.5E-03	0.6	2.1
SWP 23424	1.0	1.3E-03	4.0	5.9					

NOTES.—The mass accretion rate through disk,  $\dot{M}$ , is derived from continuum fits and has units  $1.1 \times 10^{18} \text{ g s}^{-1}$ . This quantity is constrained to be  $\leq 1$ . (2) X-ray illumination strength parameter defined in equation (2). Optical error is a measure of the disagreement between the average optical flux at 5000 Å (based on  $m_v = 13$ ) and the disk model prediction and is defined in eq. (3). The disk outer radius,  $R_{\text{max}}$ , is derived from the continuum fits and has units  $3 \times 10^{10} \text{ cm}$ .

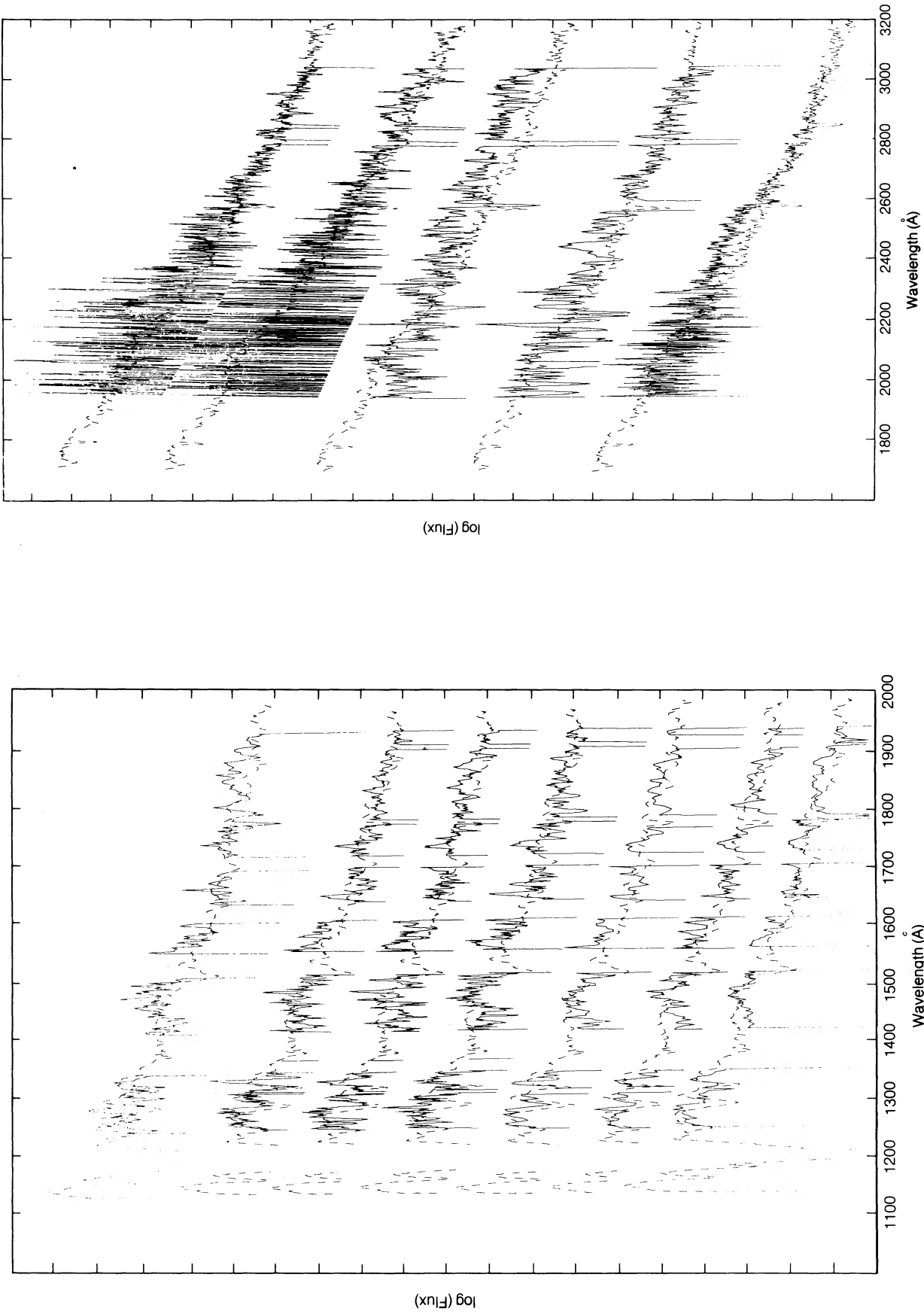


FIG. 4.—Fits of accretion disk and X-ray-illuminated accretion disk models (*dashed curves*) to the continuum (*solid curve*) after line subtraction for various spectra. Data are omitted in wavelength regions containing strong emission lines, or where cosmic-ray hits or other errors affect data quality. The various spectra correspond to those in Fig. 1.

fact that the UV is affected by the Rayleigh-Jeans turnover at  $\lambda_{\text{out}} \sim 7000 \text{ \AA}$ .

Also included as a constraint in the fits is the average optical flux at  $5000 \text{ \AA}$  (based on the average optical magnitude,  $m_v = 13$ ). A measure of the disagreement between the fitted disk spectra and the observed optical flux is provided in Table 2A as

$$\text{opt. err.} = F_{\text{disk}}/F_{\text{opt}} - 1, \quad (3)$$

where  $F_{\text{disk}}$  is the flux at  $5000 \text{ \AA}$  predicted by the best-fit model, and  $F_{\text{opt}}$  is the approximate observed flux. The best-fit values of this quantity are generally greater than zero, reflecting the fact that the disk models tend to overproduce the optical relative to what is observed. Possible explanations for this fact include the fact that we have adopted a crude measure of  $F_{\text{opt}}$ , and the true value may differ from this by up to 1 magnitude (e.g., Willis et al. 1980). However, we consider our value to be no less reliable than the use of the *IUE* fine error sensor (FES) measurements, since these require a bolometric correction which is uncertain for Sco X-1, and since the reporting of FES measurements has not been done consistently by the many different observers responsible for obtaining the Sco X-1 data. Another possible source of the discrepancy lies in the extrapolation of our model spectra to wavelengths greater than  $3600 \text{ \AA}$  since the observed Balmer jump is not adequately reproduced by our models. We have also tried fits in which the constraint of minimum opt. err. is omitted; the results differ little ( $\leq 5\%$ ) from those given in Table 2A for short-wavelength spectra. Long-wavelength spectral fits calculated without the optical flux constraints have  $\dot{M}$  values generally greater than those in Table 2A by up to 20%, while the  $f_x$  values are affected by less than 2%.

Blair et al (1984) interpreted the UV emission of Cen X-4 with models of X-ray-heated accretion disks based on the assumption that the X-rays travel radially from the central compact object to each element of disk surface. Vrtilek et al. (1989, 1990) improved these models and used them to fit spectra of Cyg X-2 and the 1989 observations of Sco X-1. Our treatment is based on the hypothesis that the X-rays pass through and are scattered by corona above the disk. These are clearly the two extreme assumptions. There is strong observational evidence for the existence of accretion disk coronae comparable in size to the disk based on the light curves of edge-on systems (White & Holt 1982), but the faintness of these systems suggests that less than  $\sim 10\%$  of the X-rays are scattered. Observational knowledge of coronal structure and scattering properties on smaller scales is very limited. Thus we hope that, as usual, the truth lies between the two extremes.

It would be desirable to determine the nature of the accretion disk corona from the reprocessed X-ray radiation which emerges in the UV and optical, but this is not practical. The difference between the two extreme models comes down in the end to a dependence on the angle between the disk surface and the rays from the central object in the direct illuminations case, and the lack of such a dependence in the coronal case. While it is clear from the results of our fits and of those of Vrtilek et al. (1990) that the X-ray heating exceeds the viscous heating of the disk by an overwhelming margin, Vrtilek et al. (1990) predict that the temperature varies as  $R^{-3/7}$  while the uniform illumination model gives  $T \sim R^{-1/2}$ . Given the primitive state of our understanding of the detailed emission spectrum from the disk and our lack of knowledge of  $R_{\text{out}}$  or the X-ray albedo, these radial temperature structures are essentially identical.

We have explored the consequences of our assumption

about the local disk radiation spectrum by performing fits which use blackbody spectra rather than stellar atmospheres; these require less disk heating (viscous or X-ray illumination) in order to explain the observations than do stellar atmosphere models, owing to the more efficient emission in the blackbody case. However, the differences between the two sets of fits are less than the dispersion among the various fits of one set or the other, so we deem them unimportant. We note that the product  $f_x \dot{M} R_{\text{max}}^2$  basically gives the total UV and optical luminosity and therefore, given the assumed distance, it is the quantity derived from the UV and optical brightness level. The separation of the product into the three factors is far more uncertain. It depends on matching the spectral slope and, therefore, on the accuracy of the assumed intrinsic emission spectra. The limitations of this separation can be seen from the systematic differences in  $\dot{M}$  and  $f_x$  determined from the long-wavelength and short-wavelength spectra in Table 2A. Much of this difference may result from the lack of a meaningful treatment of the Balmer continuum. The Balmer jump is absent in the blackbody models, is a strong absorption feature in the models based on stellar spectra, and is a strong emission feature in actual observations (e.g., Schachter et al. 1989).

#### 2.4.2. Lines

Emission-line strengths were extracted by fitting the spectra in the vicinity of emission lines to a linear continuum plus a Gaussian line or blend of (two) lines. This procedure was carried out for each individual image and for the averaged spectra for the obvious strong lines: N v  $\lambda 1240$ , O v  $\lambda 1370$ , Si iv  $\lambda 1400$ , C iv  $\lambda 1550$ , He II  $\lambda 1640$ , and N iv  $\lambda 1718$ . This procedure allows for the doublet structure of the Si iv and N v lines. Hydrogen Ly $\alpha$  is assumed to be contaminated by geocoronal emission; its profile was fitted together with the fits to N v  $\lambda 1240$ . We have not included absorption in our fits to the Ly $\alpha$  line. Tables 2B and 2C present the line fluxes (in units of  $10^{-11} \text{ ergs s}^{-1} \text{ cm}^{-2}$ ), equivalent widths (in  $\text{\AA}$ ), and the fractional errors associated with these quantities.

#### 2.5. Correlations

In order to better understand the variability behavior of the Sco X-1 UV spectrum we have searched the results of our spectral fits for correlations between the various different quantities: line strengths, the continuum in the vicinity of the lines, the global continuum parameters ( $\dot{M}$ ,  $f_x$ , and  $R_{\text{out}}$ ), the optical brightness at the time of the UV observations, the epoch of the observations, and the orbital phase. We have done this by testing all of the various pairs of columns in Tables 1 and 2 for linear correlations and using linear regression as well as the nonparametric correlation coefficients of Spearman and Kendall (see, e.g., Press et al. 1986).

We find correlations between the fluxes of most of lines and their continua, in the sense that the equivalent widths remain approximately constant with intensity. These are illustrated in Figure 5. The best example is the C iv  $\lambda 1550$  line, whose flux and adjacent continuum are linearly correlated with a coefficient of 0.84 and an error less than or equal to 0.1; He II  $\lambda 1640$  and Si iv  $\lambda \lambda 1397, 1403$  exhibit similar behavior, although at a lower level of significance. Also, the continua under the emission lines are all correlated with the parameter  $\dot{M}$ . These correlations are apparent in all the various statistical tests employed, and the probability of these correlations occurring at random (under the assumption that the relevant statistic is normally distributed) is low ( $\leq 0.01$ ). Thus, the continuum shape and line equivalent widths are approximately constant

TABLE 2B  
DERIVED LINE STRENGTHS

IMAGE NUMBER	1240				1370				1398			
	$F_{\text{line}}$	$\sigma$	EW	$\sigma$	$F_{\text{line}}$	$\sigma$	EW	$\sigma$	$F_{\text{line}}$	$\sigma$	EW	$\sigma$
SWP 1444	17.9	0.02	12.6	2.2	1.3	0.5	1.10	0.50	8.6	0.04	8.0	0.88
SWP 1452	18.1	0.04	9.46	1.3	2.7	0.2	1.77	0.42	9.3	0.04	6.7	0.72
SWP 1463	19.4	0.03	11.9	2.0	2.4	0.2	1.83	0.37	9.0	0.04	7.7	0.82
SWP 1470	19.0	0.05	8.62	0.9	3.2	0.2	1.78	0.39	11.	0.04	6.8	0.74
SWP 1473	17.7	0.05	7.74	1.2	3.2	0.3	1.73	0.51	9.3	0.04	5.6	0.65
SWP 1490	18.4	0.04	9.64	1.5	1.3	0.7	0.80	0.58	11.	0.03	8.1	0.95
SWP 1491	12.5	0.07	6.24	0.9	1.9	0.4	1.16	0.51	9.6	0.04	6.7	0.76
SWP 1499	14.1	0.07	6.64	0.8	3.0	0.2	1.78	0.39	8.1	0.05	5.3	0.59
SWP 1953	4.49	0.23	2.50	0.6	1.3	0.5	0.89	0.41	7.7	0.05	6.0	0.73
SWP 2028	38.3	0.03	12.5	2.4	6.4	0.2	2.26	0.43	15.	0.05	5.8	0.68
SWP 2033	18.3	0.04	9.47	1.6	3.5	0.2	2.00	0.42	11.	0.04	7.2	0.86
SWP 2039	34.8	0.03	15.9	2.0	3.8	0.2	1.86	0.42	9.8	0.06	5.4	0.65
SWP 2040	21.5	0.04	10.9	1.7	5.0	0.1	2.79	0.42	15.	0.03	9.5	1.03
SWP 2041	37.8	0.03	14.6	1.9	6.3	0.1	2.61	0.38	14	0.05	6.6	0.78
SWP 2048	16.0	0.05	7.70	1.3	3.3	0.2	1.75	0.42	13.	0.04	7.7	0.89
SWP 2062	14.3	0.04	10.9	2.0	1.5	0.3	1.22	0.41	7.3	0.05	6.7	0.73
SWP 2063	10.5	0.05	9.27	1.3	1.6	0.3	1.48	0.45	6.5	0.04	6.9	0.75
SWP 2064	12.3	0.04	10.3	1.7	1.2	0.4	1.12	0.41	7.7	0.04	7.8	0.93
SWP 2065	9.83	0.06	7.56	1.2	1.0	0.5	0.85	0.45	6.6	0.05	6.0	0.69
SWP 2066	11.9	0.04	9.46	1.4	1.3	0.3	1.15	0.38	4.9	0.07	4.7	0.61
SWP 2076	8.63	0.06	6.49	1.0	1.0	0.5	0.87	0.41	5.2	0.07	4.9	0.58
SWP 2077	10.9	0.05	8.06	1.3	1.6	0.3	1.30	0.41	8.8	0.04	8.1	0.90
SWP 2078	15.5	0.03	12.0	2.2	0.7	0.8	0.59	0.50	9.1	0.03	8.7	1.01
SWP 2079	3.90	0.22	2.04	0.5	0.3	2.8	0.21	0.58	6.3	0.07	4.5	0.57
SWP 2080	7.17	0.09	5.07	0.9	1.2	0.4	1.04	0.45	4.9	0.07	4.7	0.61
SWP 4641	32.7	0.04	10.3	1.1	6.4	0.2	2.41	0.40	14.	0.05	6.0	0.69
SWP 4642	13.9	0.06	7.56	1.1	1.9	0.3	1.25	0.41	10.	0.04	7.6	0.84
SWP 7782	50.4	0.03	16.6	2.3	4.8	0.3	1.70	0.46	17.	0.04	6.7	0.77
SWP 8744	25.6	0.04	9.37	1.5	1.9	0.5	0.84	0.45	11.	0.06	5.5	0.65
SWP 9636	23.7	0.06	7.28	0.8	4.0	0.3	1.46	0.41	12.	0.06	4.9	0.62
SWP 9658	1.93	0.48	1.21	0.6	0.3	2.6	0.23	0.58	6.0	0.06	5.4	0.67
SWP 22424	9.49	0.63	5.51	0.6	2.4	0.2	1.68	0.32	7.1	0.04	5.6	0.50
SWP 22453	11.3	0.41	4.69	0.5	3.2	0.2	1.64	0.32	7.9	0.05	4.6	0.43
SWP 22485	8.72	0.19	4.28	0.5	2.3	0.2	1.38	0.34	7.8	0.04	5.3	0.47
SWP 22486	11.8	0.54	8.38	0.5	4.9	0.1	2.42	0.29	11.	0.04	6.3	0.56
SWP 22512	27.0	0.05	6.80	0.7	8.2	0.1	2.54	0.31	17.	0.04	5.8	0.50
SWP 22513	28.4	0.04	7.22	0.7	6.5	0.1	2.02	0.31	17.	0.04	5.8	0.50
SWP 22514	22.9	0.06	5.59	0.6	6.4	0.2	1.93	0.33	16.	0.04	5.5	0.51
SWP 23424	23.3	0.04	8.32	1.1	7.8	0.1	3.46	0.33	10.	0.04	5.2	0.46
SWP 23425	26.0	0.03	9.10	1.1	6.5	0.1	2.84	0.28	13.	0.03	6.4	0.52
SWP 23479	26.6	0.02	12.2	1.0	3.1	0.2	1.59	0.31	12.	0.03	7.1	0.61
SWP 23480	30.9	0.02	14.3	1.1	3.7	0.2	1.91	0.33	13.	0.03	7.6	0.64
SWP 23592	34.2	0.03	11.3	1.4	6.1	0.1	2.44	0.29	18.	0.03	7.9	0.65
SWP 23593	31.0	0.03	10.6	1.3	3.7	0.2	1.53	0.32	13.	0.04	5.9	0.52
SWP 23594	29.7	0.03	10.2	1.2	2.8	0.3	1.14	0.32	13.	0.04	6.1	0.54
SWP 23702	7.24	0.06	4.96	0.5	5.0	0.1	4.24	0.32	6.2	0.04	6.0	0.45
SWP 23703	9.01	0.05	5.80	0.6	1.8	0.2	1.44	0.32	5.0	0.05	4.6	0.42
SWP 23704	9.06	0.06	5.45	0.5	2.3	0.2	1.70	0.34	5.2	0.06	4.4	0.45
SWP average	16.8	0.04	8.15	1.3	3.4	0.2	1.89	0.32	10.	0.04	6.3	0.69

NOTES.—The line flux,  $F_{\text{line}}$ , is in units  $10^{-11}$  ergs  $\text{s}^{-1}$   $\text{cm}^{-2}$ . The line flux error,  $\sigma$ , is derived from Gaussian fitting to data and is expressed as a fraction of  $F_{\text{line}}$ . The line equivalent width, EW, is in angstroms. The line equivalent width error is derived from line flux error and linear continuum fitting to data and is expressed as a fraction of EW.

over the measured range of intensities, which is approximately a factor of 3.

We also find correlations which imply departures from the simple scaling of the continuum strength and line flux with intensity: The lines arising from the most highly ionized ions vary faster with continuum intensity than do those from moderate charge. Figure 5 displays the most notable example of this behavior, that of O v  $\lambda 1370$ , relative to the continuum at C iv  $\lambda 1550$ . The constant of proportionality in this case is 2.82, the coefficient of linear correlation is 0.73, and the error on the coefficient is less than or equal to 0.1. The N v  $\lambda 1240$  line behaves similarly.

We find no significant correlations between orbital phase or

observing epoch and any of our other measured or derived quantities. We set an upper limit of 10% for modulation at the orbital period of the emission lines and adjacent continua. Thus we find no evidence for an association of UV emission (or absorption) and the secondary star in Sco X-1, and no evidence of secular trends in the UV emission over the 6 yr spanned by these data.

We are unable to detect any significant correlations between the various parameters which characterize our continuum fits. Two of these parameters,  $R_{\text{max}}$  and  $f_x$ , can both influence the model continuum at the longest wavelengths. It is therefore possible that these can “beat” against each other, leading to a larger dispersion in the fitted values than is present in the data

TABLE 2C  
 DERIVED LINE STRENGTHS

IMAGE	1549				1640				1718			
	$F_{\text{line}}$	$\sigma$	EW	$\sigma$	$F_{\text{line}}$	$\sigma$	EW	$\sigma$	$F_{\text{line}}$	$\sigma$	EW	$\sigma$
SWP 1444	27.8	0.007	31.0	8.9	4.4	0.04	5.4	0.40	3.2	0.06	4.5	0.41
SWP 1452	32.5	0.008	28.1	7.0	3.9	0.10	3.7	0.43	3.2	0.10	3.3	0.39
SWP 1463	27.0	0.009	27.7	7.8	3.1	0.11	3.4	0.43	3.4	0.08	4.4	0.51
SWP 1470	33.0	0.009	24.9	5.3	5.5	0.05	4.6	0.32	2.7	0.12	2.6	0.32
SWP 1473	43.5	0.007	31.5	7.5	6.2	0.07	4.9	0.50	4.2	0.09	3.9	0.47
SWP 1490	35.0	0.007	30.4	7.3	4.2	0.08	4.1	0.46	3.2	0.09	3.4	0.38
SWP 1491	23.3	0.015	18.8	3.3	12.	0.03	11.	1.44	1.7	0.25	1.8	0.46
SWP 1499	30.4	0.009	23.9	4.2	5.7	0.05	5.0	0.33	3.5	0.09	3.5	0.37
SWP 1953	26.1	0.01	24.4	5.8	3.4	0.09	3.5	0.36	1.6	0.22	1.8	0.42
SWP 1954	22.6	0.014	20.8	4.3	3.6	0.10	3.6	0.42	2.0	0.16	2.3	0.38
SWP 2028	40.6	0.014	19.2	3.8	3.9	0.25	2.0	0.51	5.3	0.10	3.1	0.34
SWP 2033	36.6	0.01	28.5	9.1	5.6	0.07	4.8	0.45	2.6	0.15	2.5	0.43
SWP 2039	41.0	0.011	27.9	9.2	6.1	0.08	4.4	0.46	3.6	0.12	2.9	0.40
SWP 2040	40.8	0.009	30.9	11.	4.0	0.11	3.3	0.42	4.7	0.08	4.3	0.54
SWP 2041	49.2	0.011	28.0	9.1	5.6	0.10	3.4	0.38	3.7	0.14	2.6	0.38
SWP 2048	50.0	0.007	35.7	14.	6.2	0.07	4.9	0.46	2.3	0.17	2.1	0.37
SWP 2062	25.1	0.011	28.5	10.	3.5	0.08	4.4	0.44	3.4	0.06	4.8	0.46
SWP 2063	19.9	0.012	25.8	8.2	3.7	0.05	5.2	0.43	0.9	0.36	1.4	0.51
SWP 2064	27.0	0.009	32.9	13.	3.0	0.08	4.0	0.41	1.1	0.24	1.7	0.42
SWP 2065	23.6	0.009	26.1	7.0	1.9	0.18	2.3	0.42	2.1	0.10	2.9	0.35
SWP 2066	31.6	0.007	36.0	14.	3.1	0.10	3.9	0.47	3.0	0.07	4.1	0.42
SWP 2076	23.1	0.011	26.8	8.3	4.1	0.06	5.3	0.53	3.4	0.06	4.9	0.51
SWP 2077	26.4	0.01	29.3	9.9	3.4	0.08	4.2	0.41	2.0	0.13	2.7	0.41
SWP 2078	28.5	0.008	32.7	11.	4.0	0.06	5.0	0.47	2.8	0.08	3.9	0.42
SWP 2079	29.1	0.011	24.6	6.0	3.4	0.11	3.1	0.38	2.9	0.13	3.0	0.42
SWP 2080	27.4	0.008	31.9	12.	3.9	0.07	5.1	0.52	3.0	0.07	4.3	0.43
SWP 4641	38.3	0.014	19.5	4.0	5.0	0.11	2.8	0.33	4.6	0.13	2.9	0.43
SWP 4642	29.3	0.01	25.5	6.7	3.2	0.09	3.1	0.30	2.7	0.13	2.9	0.44
SWP 7782	44.7	0.012	21.4	4.7	8.3	0.08	4.4	0.44	5.4	0.10	3.2	0.39
SWP 8744	37.6	0.012	23.1	6.1	2.8	0.23	1.9	0.46	4.9	0.08	3.8	0.43
SWP 9636	41.9	0.011	20.8	4.0	5.2	0.12	2.8	0.35	4.2	0.14	2.6	0.41
SWP 9658	19.6	0.013	21.7	5.3	1.2	0.31	1.4	0.45	2.0	0.14	2.9	0.45
SWP 22424	28.5	0.008	27.3	5.5	3.6	0.06	3.7	0.27	2.4	0.10	2.9	0.31
SWP 22453	31.7	0.008	22.1	3.5	2.4	0.16	1.8	0.29	2.9	0.11	2.6	0.30
SWP 22485	26.4	0.009	21.7	3.3	5.5	0.04	5.0	0.26	2.9	0.09	3.1	0.34
SWP 22486	42.8	0.007	28.4	5.2	4.5	0.07	3.2	0.24	4.0	0.08	3.3	0.32
SWP 22512	50.9	0.008	21.2	2.8	8.1	0.06	3.7	0.25	6.1	0.08	3.1	0.30
SWP 22513	51.7	0.008	21.6	3.0	9.2	0.05	4.2	0.29	6.4	0.08	3.4	0.34
SWP 22514	48.9	0.01	20.2	2.8	4.7	0.13	2.1	0.28	5.1	0.11	2.7	0.33
SWP 23424	39.7	0.008	23.7	4.1	6.5	0.05	4.2	0.28	3.5	0.11	2.6	0.33
SWP 23425	47.0	0.006	27.3	4.9	4.2	0.13	2.7	0.37	4.7	0.09	3.5	0.36
SWP 23479	47.2	0.005	32.1	7.1	5.8	0.08	4.4	0.43	3.9	0.08	3.3	0.31
SWP 23480	46.1	0.006	31.9	7.9	6.2	0.05	4.7	0.31	3.7	0.09	3.2	0.35
SWP 23592	59.8	0.005	31.8	7.1	7.4	0.06	4.3	0.34	4.8	0.09	3.2	0.33
SWP 23593	49.7	0.006	27.7	5.3	5.8	0.08	3.5	0.32	4.8	0.08	3.3	0.34
SWP 23594	48.1	0.006	26.9	4.7	3.8	0.15	2.3	0.36	5.1	0.07	3.5	0.31
SWP 23702	17.7	0.01	20.2	2.9	1.8	0.13	2.3	0.31	2.7	0.07	4.1	0.37
SWP 23703	19.2	0.009	21.1	3.0	1.2	0.25	1.4	0.36	2.4	0.09	3.4	0.34
SWP 23704	21.2	0.009	21.3	3.2	2.1	0.12	2.3	0.28	2.7	0.08	3.3	0.32
SWP average	36.1	0.008	26.6	5.4	4.8	0.07	3.9	0.33	3.5	0.10	3.2	0.37

NOTES.—The line flux,  $F_{\text{line}}$ , is in units  $10^{-11}$  ergs  $\text{s}^{-1}$   $\text{cm}^{-2}$ . The line flux error,  $\sigma$ , is derived from Gaussian fitting to data and is expressed as a fraction of  $F_{\text{line}}$ . The line equivalent width, EW, is in angstroms. The line equivalent width error is derived from line flux error and linear continuum fitting to data and is expressed as a fraction of EW.

at the longest wavelengths. We have tested for this possibility by searching for correlations between these two quantities and have found none. Furthermore, the quantity  $f_x$  is very tightly correlated with the continuum fluxes near the various lines (e.g., correlation coefficient = 0.85 for the continuum near C IV  $\lambda 1550$ ), while  $R_{\text{max}}$  is not. We have also tested for correlations between the quantity  $f_x MR_{\text{max}}^2$  and the other observables, and have found them to be less significant than those using  $f_x$  alone. This is likely a reflection of the large dispersion in the  $R_{\text{max}}$ .

### 3. DISCUSSION

In this section we will discuss some of the constraints that the UV data create for several simple models for the line emis-

sion region. We will assume that Sco X-1 consists of an X-ray-emitting neutron star in orbit with a late-type star, with a separation of  $\approx 3 \times 10^{11}$  cm (Crampton et al. 1976), and that the X-ray source is surrounded by an accretion disk. The line fluxes and ratios constrain the size, density, and degree of ionization of the emission region. The line variability behavior is related to the X-ray variability, and the continuum variability is related to the shape of the X-ray spectrum.

#### 3.1. Line Strengths

The most straightforward models for the emission line region would be collisionally ionized (e.g., Raymond & Smith 1977) or X-ray photoionized (e.g., Kallman & McCray 1982)

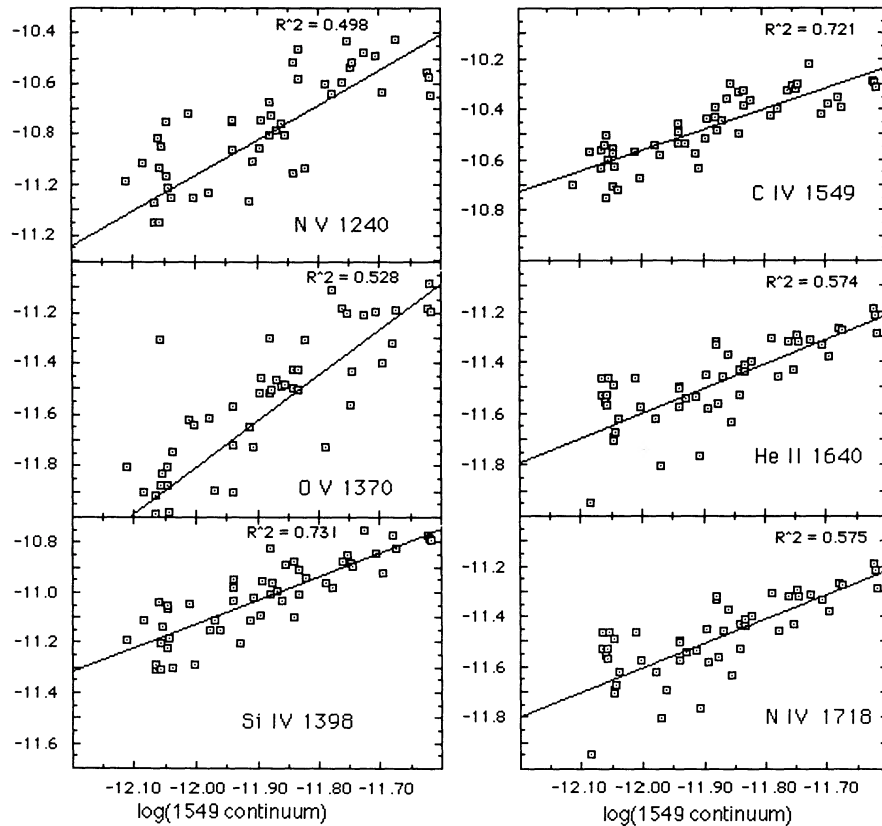


FIG. 5.—Correlation of continuum flux near the C IV emission line with line fluxes,  $F_{\text{line}}$ . Square of correlation coefficient is given as  $R^2$ .

gas which is effectively optically thin to its emission lines. The “effectively thin” assumption means that each collisional excitation is followed by the emission of a photon which may undergo a few resonant scatterings, but which eventually escapes from the emitting gas. Unfortunately, the emission lines in Sco X-1 are not effectively thin. Figure 6 shows the C IV doublet from the 540 minute high-dispersion exposure SWP 9417. The intensity ratio of the C IV  $\lambda 1550$  lines would be 2:1 in

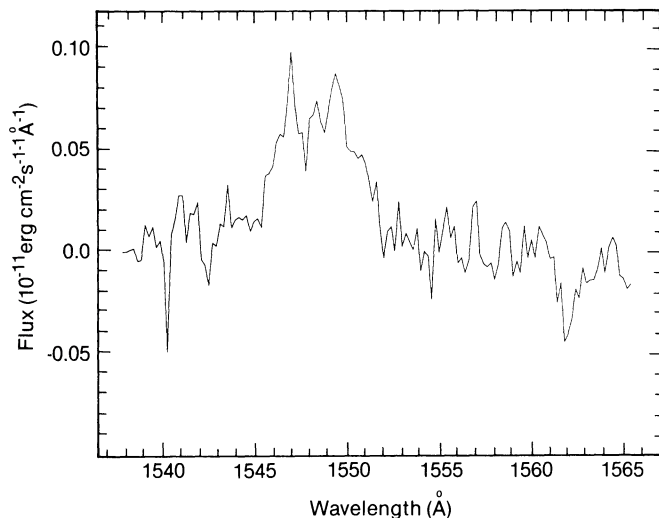


FIG. 6.—Spectrum on the vicinity of the C IV  $\lambda 1550$  line as observed at high resolution (SWP 9417).

an effectively thin gas, but it is observed to be 1:1, as expected for optically thick emission. Boyle et al. (1986) found a similar 1:1 line ratio for the N v doublet in HZ Her. The line profiles are smeared by the orbital motion of about one-half cycle during the 9 hr exposure, but this amounts to less than about  $100 \text{ km s}^{-1}$  (Crampton et al. 1976), and the roughly  $500 \text{ km s}^{-1}$  line width is consistent with the Keplerian velocity at  $5 \times 10^{10} \text{ cm}$  from a neutron star. The narrow features at  $1547.2$  and  $1549.8 \text{ \AA}$  are marginal. If real, they suggest a  $200 \text{ km s}^{-1}$  blueshifted component, possibly arising on the X-ray-heated surface of the companion star.

Interpretation of optically thick emission lines depends on radiative transfer and on geometry. Preliminary model calculations have been made employing a modified version of the code used by Mauche & Raymond (1987) for cataclysmic variable winds. That model uses an escape probability treatment to account for trapping of the spectral lines. The escape probability is computed from the smaller of the thickness of the emitting zone and the Sobolev length associated with the velocity gradient due to Keplerian shear. The calculations are uncertain owing to the simplifying assumptions made in modeling the transfer of radiation, but they show that the suppression of cooling by trapping and collisional de-excitation of lines such as C IV  $\lambda 1550$  results in a substantially higher temperature in the zone where the UV emission lines are formed, though the ionization parameter of this zone is similar to that found in the effectively thin models of Kallman & McCray (1982). The temperatures predicted are in the neighborhood of  $50,000 \text{ K}$ , and luminosities comparable to those observed (assuming a distance of  $1.4 \text{ kpc}$ ) are found. The models give N v  $\lambda 1240$  as the strongest line, followed by C IV, He II, and Si IV, in agreement

with the observed fluxes. The O v  $\lambda 1370$  line would be expected to be very weak compared with the resonance lines of C iv and N v in an optically thin gas, and it is faint or undetected in *IUE* observations of most collisionally ionized (cool star transition regions, supernova remnants) or photoionized (symbiotic stars, planetary nebulae) objects. In Sco X-1 it is one-third as strong as Si iv  $\lambda 1400$ . The optically thick models predict an intensity comparable to the Si iv line due to the trapping of resonance line photons.

### 3.2. Correlations

Support for the hypothesis that the accretion disk is the site of the UV line emission comes from the success of fits of accretion disk spectra to the continuum and from the absence of any correlation between the UV spectrum and orbital phase. Although such fits are sensitive to the assumed reddening, and although we have not tried a wide range of trial spectra, it is clear that a single-temperature blackbody would not provide an acceptable fit to the data for our choice of reddening. Therefore we will assume in what follows that the accretion disk is the reprocessor, although some of our conclusions are applicable to reprocessing by the atmosphere of the companion star.

The UV lines provide constraints on another important property of LMXB. The results of the previous section yield an upper limit of  $\Delta F/F \leq 10\%$  for variability associated with the orbital period. Using this, together with the estimate for the illumination of the accretion disk derived above,  $f_{x,disk} \approx 0.01$ , we can set a limit on the illumination of the companion star:  $f_{x,star}/f_{x,disk} \leq 0.1\Omega_{disk}/\Omega_{star} \sim 2$ , where  $\Omega$  is the solid angle subtended by the disk or star as seen by the X-ray source. The inclination of the system adds at most a factor of 2 uncertainty to this number, since we believe that  $i \approx 30$  (Crampton et al 1976). Thus the illumination of the companion star cannot greatly exceed that of the disk. Possible reasons for this include shadowing by the disk or a "bulge" at the edge of the disk. This, in turn, constrains the dynamical importance of illumination for Sco X-1. For example, it has been suggested that illumination of the companion star in LMXBs can produce a "self-excited wind" (Basko & Sunyaev 1973; London, McCray, & Auer 1981), and that such winds can have important consequences for binary evolution (Ruderman, Shaham, & Tavani 1989). If so, it is straightforward to estimate the mass flux in such a wind (cf. Begelman et al. 1983; Begelman & McKee 1983); it is  $\dot{M} \leq 10^{18} \text{ g s}^{-1} L_{38} f_{x,star} T_7^{1/2}$ , where  $T_7$  is the wind temperature in units of  $10^7$  K and the other quantities have been defined in the previous section. It should be emphasized that this is an upper limit, and the actual value is likely to be lower owing to radiative or conductive losses (Levinson & Eichler 1989) or geometric effects. This mass loss rate can be compared with the mass accretion rate required to power the X-ray source,  $\dot{M}_{acc} \approx 10^{18} \text{ g s}^{-1} L_{38}/\eta_{0.1}$ . Therefore, if  $f_{x,star} \leq 0.02$ , as is inferred from the UV variability, the evaporative mass loss rate from the companion star is not sufficient to power the X-ray source or to affect the binary evolution of Sco X-1. Similar tests, when applied to a larger sample of LMXBs, can provide a test of the importance of self-excited winds.

We expect that an atmosphere will reprocess X-rays into UV

radiation according to a crude mapping of X-ray energy into UV wavelength in a manner which is familiar from studies of stellar atmospheres: UV lines, having greater opacity, are emitted preferentially farther from the disk midplane, where the column density toward the observer, and toward the incoming X-rays, is lowest. The continuum is emitted preferentially at greater column density. Thus the lines are likely to arise from reprocessing of soft X-rays ( $\epsilon \leq 1$  keV) which are absorbed preferentially at low ( $\leq 10^{22} \text{ cm}^{-2}$ ) column densities, while the continuum represents reprocessing of hard X-rays. The time scales for the reprocessing to occur, i.e. recombination, diffusion, and light travel times across the disk, are all short compared to the interval between observations. According to this hypothesis, the observed emission lines are a probe of the soft X-ray illumination of the reprocessor, while the value of  $f_x$  which we derive from the continuum fits is a probe of the hard X-ray illumination.

These correlations have potentially important implications for the interpretation of hard X-ray observations from Sco X-1, which form the basis for most models of this object: The hard X-ray flux may not be an indicator of the mass accretion rate onto the compact object and in fact may vary inversely with  $\dot{M}$ ; soft X-rays are more likely to be such an indicator, particularly when the source is in its "normal branch" X-ray spectral state (e.g., Hasinger, Priedhorsky, & Middleditch 1989). A test of this idea is provided by the equivalent width variations: the approximate constancy of the equivalent widths of C iv and Si iv implies that the ratio of hard-to-soft X-ray flux does *not* vary strongly among the various spectra we analyzed.

The other observed correlations, those between the various emission lines, provide constraints primarily upon the conditions within the reprocessor. Although these cannot be adequately interpreted without detailed models for an illuminated atmosphere, they are consistent with our simple scenario. As described in the previous section, we find that the O v  $\lambda 1370$  and N v  $\lambda 1240$  lines vary faster than linearly with the C iv  $\lambda 1549$  line. This is the behavior expected from a gas in which the most abundant ions of a given element are of a lower stage than those producing the observed lines. In this case,  $\text{C}^{+3}$ ,  $\text{N}^{+3}$ , and  $\text{O}^{+3}$  are likely to be the most abundant ions of their respective elements. The C iv line is a good indicator of the ionizing flux incident on the gas, and therefore on the mean ionization of the gas. The variations of O v  $\lambda 1370$  and N v  $\lambda 1240$  represent the nonlinear increase of the abundances of their parent ions as the ionizing flux increases. An alternative explanation for this behavior is that it is due to changes in the shape of the ionizing spectrum. The relative merits of these explanations cannot be evaluated without detailed models for the emission region.

We would like to thank the staff of the *IUE* Regional Data Analysis Facility at Goddard Space Flight Center, and F. Verbunt and G. Reichert for consultations and advice concerning the data analysis. This research was partially supported by NASA grant NAG5-87 to the Smithsonian Astrophysical Observatory, and by NASA grant N075-88 through the Astrophysical Data Program.

### REFERENCES

- Basko, M., & Sunyaev, R. 1973, *Ap&SS*, 23, 117  
 Begelman, M. C., & McKee, C. F. 1983, *ApJ*, 271, 89  
 Begelman, M. C., McKee, C. F., & Shields, G. A. 1983, *ApJ*, 271, 70  
 Blair, W. P., Raymond, J. C., Dupree, A. K., Wu, C. C., Holm, A. C., & Swank, J. H. 1984, *ApJ*, 278, 270  
 Boggess, A., et al. 1978a, *Nature*, 275, 372  
 Boggess, A., et al. 1978b, *Nature*, 275, 377  
 Boyle, S., Howarth, I., Wilson, R., & Raymond, J. 1986, in *New Insights in Astrophysics* (Paris: European Space Agency) 471  
 Canizares, C., et al. 1975, *ApJ*, 197, 457

- Clavel, J., et al. 1990, A&A, submitted  
 Crampton, D., Cowley, A., Hutchings, J. B., & Kaat, C. 1976, ApJ, 207, 907  
 Eardley, D., Lightman, A., Payne, D., & Shapiro, S. 1978, ApJ, 224, 53  
 Gottlieb, E. W., Wright, E. L., & Liller, W. 1975, ApJ, 195, L33  
 Hasinger, G., Priedhorsky, W. C., & Middleditch, J. 1989, ApJ, 337, 843  
 Horne, K. 1985, MNRAS, 213, 129  
 Howarth, I. D., & Wilson, R. E. 1983, MNRAS, 202, 347  
 Jameson, R. F., King, A. R., & Sherrington, M. R. 1980, MNRAS, 191, 559  
 Kallman, T. R., & McCray, R. A. 1982, ApJS, 50, 263  
 Kenyon, S. 1989, private communication  
 Knude, J. 1987, A&A, 171, 289  
 Levinson, A., & Eichler, D. 1989, preprint  
 London, R. 1982, in Cataclysmic Variables and Low Mass X-ray Binaries, ed. J. Patterson & D. Lamb (Dordrecht: Reidel)  
 London, R., McCray, R., & Auer, L. 1981, ApJ, 243, 970  
 Mauche, C., & Raymond, J. 1987, ApJ, 323, 690  
 Press, W., Flannery, W., Teukolsky, S., & Vetterling, W. 1986, Numerical Recipes, (Cambridge: Cambridge University Press)  
 Raymond, J. C., & Smith, B. H. 1977, ApJS, 35, 419  
 Ruderman, M., Shaham, J., & Tavani, M. 1989, ApJ, 336, 507  
 Savage, B. D., & Mathis, J. S. 1979, ARAA, 17, 73  
 Schachter, J., Filippenko, A. V., & Kahn, S. M. 1989, ApJ, 340, 1049  
 Shakura, N. I., & Sunyaev, R. A. 1973, A&A, 24, 337  
 Shaviv, G., & Wehrse, H. 1986, A&A, 159, 15  
 Urry, C. M., & Reichert, G. A. 1989, IUE Newsletter, 34, 95  
 Vrtilak, S. D., Raymond, J. C., Verbunt, F., & Penninx, W. 1989, A&A, in press  
 Vrtilak, S. D., et al. 1990, ApJ, submitted  
 Wade, R. A. 1984, MNRAS, 208, 381  
 White, N. E., & Holt, S. S. 1982, ApJ, 257, 318  
 White, N. E., Stella, L., & Parmar, A. 1988, ApJ, 324, 363  
 Willis, A., et al. 1980, ApJ, 237, 596